



## Nocturnal temperature structure in the mesopause region over the Arecibo Observatory (18.35°N, 66.75°W): Seasonal variations

Jonathan S. Friedman<sup>1</sup> and Xinzhao Chu<sup>2</sup>

Received 3 November 2006; revised 6 May 2007; accepted 8 June 2007; published 31 July 2007.

[1] We present the mean seasonal climatology of the nocturnal temperature structure in the mesopause region (80–105 km) above the Arecibo Observatory, Puerto Rico (18.35°N, 66.75°W) from 106 nights of potassium Doppler lidar observations between December 2003 and September 2006. This first complete range-resolved mesopause climatology for a tropical latitude exhibits several unique features. Compared to higher latitude sites, mesospheric temperature inversion layers in the nocturnal means are much weaker at Arecibo. Seasonally large inversions occur in summer but are almost non-existent during the rest of the year. The Arecibo climatology shows a three-level mesopause: a high altitude in summer (~100 km), a medium altitude in late autumn and winter (~96 km), and a low altitude in early spring (~91 km). The mesopause is cold in the solstices (~171 K in summer, ~176 K in winter) and warm around equinoxes, particularly late autumn when it is near 195 K, while the spring mesopause temperature is close to 185 K. The lower thermosphere around 100 km at Arecibo shows a decreasing temperature from spring to summer when it reaches its coldest temperature, which is contrary to the increasing temperature observed at all midlatitude locations. Semiannual variations in the seasonal temperature have amplitudes as large as the annual variations through most of the MLT altitude range at Arecibo. These observed seasonal variations appear to be associated with the semi-annual oscillation, a predominantly tropical phenomenon. This report provides one of the very few observations of the semi-annual oscillation in lower thermosphere temperature.

**Citation:** Friedman, J. S., and X. Chu (2007), Nocturnal temperature structure in the mesopause region over the Arecibo Observatory (18.35°N, 66.75°W): Seasonal variations, *J. Geophys. Res.*, *112*, D14107, doi:10.1029/2006JD008220.

### 1. Introduction

[2] Many radiative, chemical and dynamic processes play important roles in determining the thermal structure of the middle atmosphere [Roble, 1995; Garcia, 1989]. The mean background temperature is largely determined by radiative forcing, which mainly includes the heating associated with absorption of solar UV radiation by O<sub>3</sub> and O<sub>2</sub> [Mlynczak and Solomon, 1993], and radiative cooling associated with infrared emissions of CO<sub>2</sub> [Andrews *et al.*, 1987]. Chemical heating from exothermic reactions contributes energy to the middle atmosphere while energy may be lost from the atmosphere by airglow from excited photolysis products or by chemiluminescent emission from product species of exothermic chemical reactions [Riese *et al.*, 1994]. Dynamical forcing strongly influences the global structure of upper mesospheric temperatures. Momentum deposited by breaking gravity waves in the summer mesopause region slows down or reverses the zonal winds, resulting in a

strong mean meridional circulation [Lindzen, 1981; Holton, 1982]. Strong upwelling at the summer pole, strong downwelling at the winter pole, and a summer-to-winter meridional flow at intermediate latitudes, associated with this single-cell meridional circulation, produce significant departures from radiative equilibrium through adiabatic heating and cooling at the high and mid latitudes [Garcia and Solomon, 1985]. At low latitudes, seasonal variation in the zonal winds produces a semiannual oscillation (SAO) [Groves, 1972; Sassi and Garcia, 1997; Garcia *et al.*, 1997], which is reflected in wind, temperature, and airglow intensity measurements [Clancy and Rusch, 1989; Takahashi *et al.*, 1995; Taylor *et al.*, 2005; Shepherd *et al.*, 2006]. In spite of the current depth of understanding of middle atmospheric chemistry, energetics, and dynamics, it is still difficult to accurately model the dynamical, radiative, and chemical forcing in the mesosphere and lower thermosphere (MLT) region, partly owing to the paucity of high-accuracy and high-resolution data of the important parameters (such as temperature and wind) in this region.

[3] Observations of the MLT thermal structure are essential for understanding the atmospheric energetics and dynamics and for validating and calibrating atmospheric general circulation models. Groundbased lidars, especially the resonance fluorescence lidars, have made great contributions in the measurement of MLT temperatures and the

<sup>1</sup>NAIC Arecibo Observatory, Arecibo, Puerto Rico, USA.

<sup>2</sup>Cooperative Institute for Research in Environmental Sciences & Department of Aerospace Engineering Sciences, University of Colorado, Boulder, USA.

study of atmospheric dynamics (see a summary by *Chu and Papp* [2005]). In particular, measurements of MLT temperatures throughout the year are extremely valuable as they provide important insight on seasonal variations and sensitive tests of large-scale dynamics of the middle atmosphere. For example, lidar observations in the Arctic and Antarctic have shown the significant departures of MLT thermal structure from radiative equilibrium due to dynamics as discussed above, that is., the mesopause temperature in summer is more than 60 K colder than in winter at these high latitudes [*Lübken and von Zahn*, 1991; *Pan and Gardner*, 2003; *Kawahara et al.*, 2004]. Better global distribution of high-quality measurements by resonance Doppler lidars is prompting critical refinements of sophisticated general circulation and wave models [e.g., *Pan et al.*, 2002; *Kawahara et al.*, 2002]. These refinements require long-term, high quality, and geographically disperse data sets for both input to (such as gravity wave parameterizations) and output from (such as seasonal thermal structure and the magnitudes of tidal modulations) those models. Such long-term, high-frequency, year-round measurements have been achieved at mid latitudes at Fort Collins (41°N, 105°W), Urbana (40°N, 88°W), and Starfire Optical Range (35°N, 106.5°W) [e.g., *She et al.*, 2000; *Chen et al.*, 2000; *States and Gardner*, 2000a; *Chu et al.*, 2005] and in the high latitudes at the South Pole (90°S), Syowa (69°S, 39°E), and Andoya (69°N, 16°E) [e.g., *Pan and Gardner*, 2003; *Kawahara et al.*, 2004; *Lübken and von Zahn*, 1991].

[4] The MLT thermal structure at low-latitude is expected to be significantly different from those at mid and high latitudes due to the different strengths of the vertical motions associated with the meridional circulations at different latitudes. However, year-round, high quality and quantity measurements are still very rare at low latitudes (from 23°N to 23°S). Satellite observations have produced some results [e.g. *Shepherd et al.*, 2004, 2005]. These are limited in local time and altitude resolution by orbital and instrument parameters and must be supplemented by geographically distributed, long-term and comprehensive ground-based measurements. Among six lidar measurements reported for the low latitudes, three reports were for only a few nights [*Gardner et al.*, 1995; *Clemesha et al.*, 1999; *von Zahn et al.*, 1996]. The measurements made by *Leblanc et al.* [1998] covered an entire year at Mauna Loa (19.5°N, 155.6°W), however, the Rayleigh lidar used in that study could not provide temperatures above 85 km. The climatology of MLT temperatures reported by *Friedman* [2003] was based on initial results of potassium Doppler lidar measurements at Arecibo (18.35°N, 66.75°W) from April 2001 to February 2003. These contained significant gaps in the seasonal coverage, and our later analyses found that some of these data suffered instrumental or data processing problems, leading to unreliable data quality and resulted in a marginally useful climatology assessment. High-quality temperature measurements in the MLT region (80–105 km) were made at Maui (20.7°N, 156.3°W) by a Na wind and temperature lidar on a campaign basis from January 2002 through January 2004 for the Maui/MALT campaign [*Chu et al.*, 2005]. Unfortunately, data for only four months were reported, and merely three additional months of data have been collected since. While significant differences between Maui and midlatitude thermal struc-

tures were identified in these four months of data [*Chu et al.*, 2005], the lack of year-round data prevented a comprehensive assessment of the MLT seasonal variations in the low latitudes. High-quality data with extensive seasonal coverage are greatly needed to verify theoretical predictions and to improve our understanding of forcing mechanisms in the tropical MLT region.

[5] Since the publication of *Friedman* [2003], we have made significant improvements to the Arecibo K Doppler lidar, both in the instrument and in the data processing. High fidelity in accuracy and precision is now seen in the K lidar temperature data. In addition, more extensive data sets have been collected at Arecibo since the principal system improvements were completed in December 2003. In light of these changes and the demanding need for low-latitude climatology stated above, we perform an in-depth systematic study of the nocturnal MLT thermal structure at the Arecibo Observatory. Over 700 hours of high-quality K lidar data collected from December 2003 to September 2006 are used to characterize this seasonal climatology. These results are then compared to nocturnal lidar measurements at Starfire Optical Range (SOR) and Maui [*Chu et al.*, 2005] in order to characterize the seasonal and latitudinal similarities and differences in temperature structures among the tropical site Arecibo (18.35°N), the sub-tropical site Maui (20.7°N), and the midlatitude site SOR (35°N) through the MLT region. It also helps to bring the Arecibo MLT thermal structure into the global picture.

## 2. Methodology

[6] As mentioned earlier, the high fidelity of the Arecibo temperature data comes from significant improvements on two fundamental aspects of the lidar: instrument performance and data processing. This section describes these improvements. A detailed description of the lidar operations is not given in this discussion. For this the reader is referred to a previous publication [*Friedman et al.*, 2003], which describes the lidar in detail and is not greatly affected by the changes presented here. Instrument performance improvements include modifications to both the transmitter and receiver systems that improve the spectral purity of the laser output and linearity of the detection system. In the data processing, we have improved the precision with which reliable temperatures can be extracted near the layer edges where resonance signal is weak. We have also applied new methods of averaging and binning data in deriving monthly and annual means as well as the seasonal climatology.

### 2.1. Instrument Improvements

[7] A system block diagram of the Arecibo K Doppler lidar is given in Figure 1 to illustrate the instrument improvements and for the simplicity of explanation. The dashed box on the left side contains the lidar transmitter: a pulsed alexandrite laser injection-seeded by an external cavity diode laser, along with numerous diagnostic instruments. The dashed box on the right consists of the lidar receiver and data acquisition system. Lying in the middle is the system trigger control for coordinating the transmitter and receiver synchronization. Major improvements to the original system were achieved in three areas: (1) prevention of nonlinear detector response caused by strong scattering

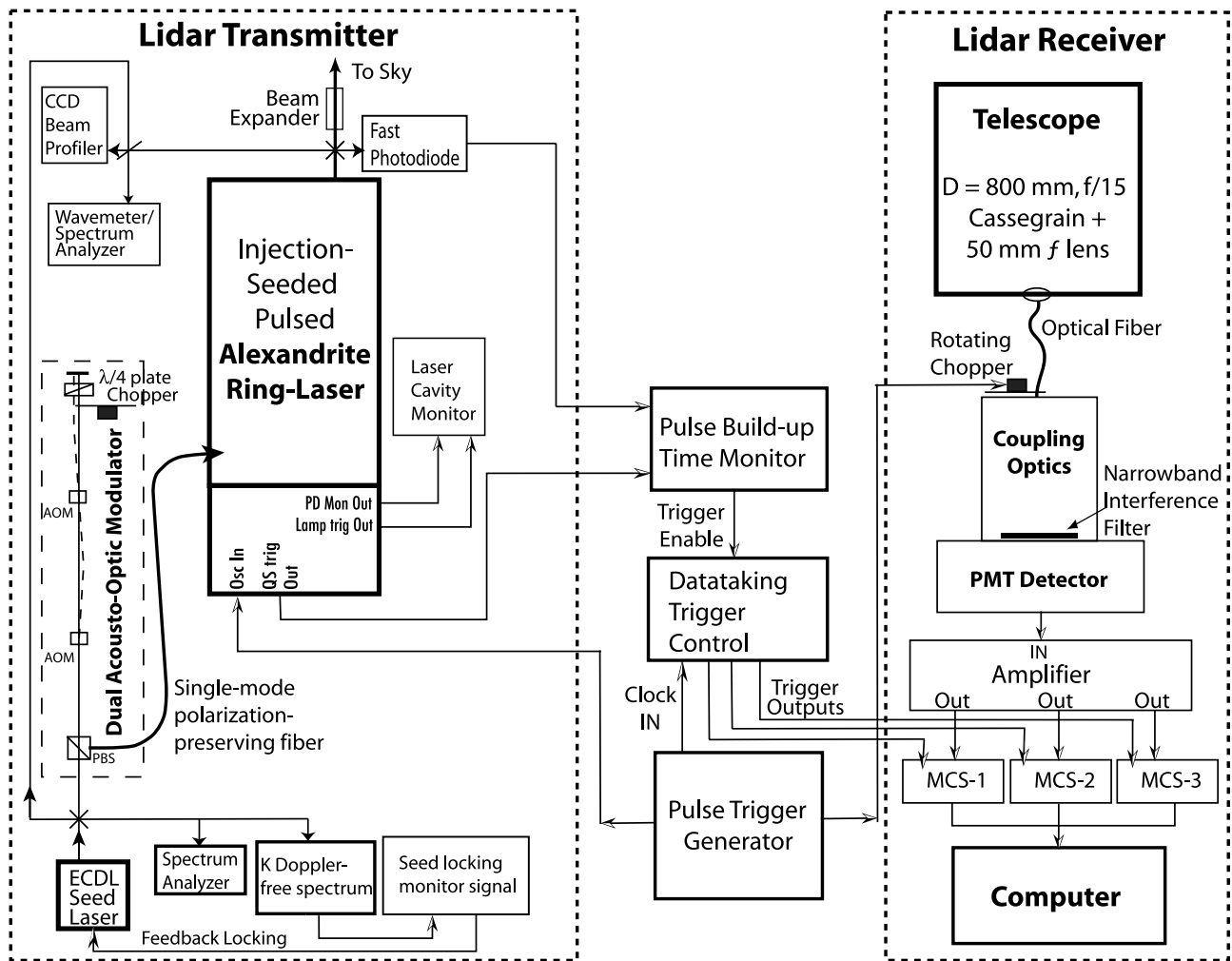


Figure 1. System diagram for the improved nighttime K Doppler lidar at Arecibo.

from low altitudes; (2) assuring injection seeding by a single frequency, with no broadband or secondary frequencies bleeding in; and (3) discrimination against spectrally “bad” pulses from the transmitter laser. Below we explain the way that we have achieved these urgent improvements to the lidar system.

### 2.1.1. Lidar Receiver

[8] Due to the strong Mie and Rayleigh scattering from the lower atmosphere, the scattered light intensity from the first 20 km is quite high. In order to maximize the detection efficiency for optimum measurements from the K layer, high sensitivity photon counting detectors are used. Strong photon counts from lower altitudes can thus exceed the dynamic range of this PMT detector (a few  $\times 10^6$ ). Electronic gating was originally used to prevent PMT saturation from lower atmosphere photon returns. However, electronic gating does not actually prevent photons from impacting the photocathode and momentarily saturating its response. Such saturation may produce a nonlinear background noise level that is difficult to eliminate, and which results in a positive bias in the temperature measurement, particularly where the resonance signal is weak near the layer edges. To solve this problem, we replaced the electronic gating with a rotating-wheel chopper (see the right dashed box in Figure 1). The

chopper is phase-locked to a harmonic of the laser repetition rate to physically block low-altitude scattered light. The chopper is phased so that signal below  $\sim 15$  km is completely blocked, and above 30 km it is completely open. The successful implementation of the rotating chopper to the lidar receiver eliminates PMT saturation and flattens the noise background in recorded lidar data.

### 2.1.2. Lidar Transmitter

[9] On the transmitter side, all improvements were undertaken in order to assure single-longitudinal-mode output with no broadband or unseeded pulses from the pulsed alexandrite ring laser. A 3-frequency technique is used in the Arecibo K Doppler lidar, where two wing frequencies are generated by frequency modulating the injection seed laser with a dual-channel, two-pass acousto-optical modulator (AOM) [Arnold and She, 2003; Friedman et al., 2003]. Because the one-way conversion efficiency of an AOM is  $>85\%$ , about 2% of the double-passed seed light that is not frequency shifted can be injected into the alexandrite laser. Without blocking the unshifted laser in the original system, both shifted and unshifted seed light have been injected into the alexandrite laser. Although the unshifted seed intensity was much smaller than the shifted intensity, its presence in the alexandrite laser cavity produces unwanted output at the

unshifted seed frequency. The actual amount of unshifted output from the alexandrite is difficult to either measure or control, but in any amount it causes higher than expected photon returns when the laser is tuned to either wing frequency, which results in artificially high temperatures. To solve this problem, a specially designed chopper was implemented in the AOM path (see the left dashed box in Figure 1). The chopper is phase locked to the half laser repetition rate so that it successfully blocks the unshifted seed light when one or the other AOM is turned on.

[10] Another improvement was to remove spectrally “bad” laser pulses from the data recording. These bad pulses are caused by two principal factors. First, the original seed laser was susceptible to electrical noise and mechanical vibrations that caused the unreliable locking of the seed laser frequency to the Doppler-free feature of the potassium spectrum (for a description, see *Friedman et al.* [2003]). Second, the alexandrite laser is occasionally improperly seeded due to uncompensated drift of the laser cavity. These two effects produce spectrally broad laser pulses that artificially raise temperatures. In order to mitigate the first of these problems, in February 2002 we replaced the original seed laser with a new seeder that is far more stable than its predecessor. The second problem required a more extensive approach. Several instruments, e.g., a spectrum analyzer, a fast photodiode, and a CCD beam profiler (see the left dashed box in Figure 1), were used to monitor the laser pulses in the spectral, temporal, and spatial domains to ensure proper performance of the laser transmitter system during laser operation. A reliable measure of optimum laser spectral performance is in the “build-up time,” i.e., the time between when the laser pulse is triggered and when the light pulse is emitted. A shorter build-up time implies better spectral quality. Adding a “pulse build-up time monitor” system (see the middle part in Figure 1) is thus an extremely simple way to ensure that we record data only from spectrally high-quality laser pulses. This monitor recognizes pulses that are “late”, and consequently not reliably seeded and, if necessary, blocks the trigger to the data recording system to reject data produced by these spectrally bad pulses. With these improvements, only data produced by spectrally “good” pulses are recorded in the data acquisition system. This has dramatically improved the data quality.

## 2.2. Data Processing Methodology

[11] In the data processing, we have improved the removal of Rayleigh scattering signals from the K layer range, so as to negate their effects on the computed temperatures. The original data processing applied a simplistic approach to subtracting the Rayleigh signal, which tended to underestimate the Rayleigh signal in the K layer range and to lead to artificially high temperatures, especially near the K layer edges. We now utilize the fact that the Rayleigh signal, used to normalize the resonance signal, is proportional to the atmospheric density, i.e.,

$$\frac{N_R(z_K)}{N_R(z_R)} = \frac{n_A(z_K)}{n_A(z_R)}, \quad (1)$$

where  $N_R(z_K)$  and  $N_R(z_R)$  are the Rayleigh photon counts at the K layer altitude  $z_K$  and the Rayleigh normalization

altitude  $z_R$ , while  $N_A(z_K)$  and  $N_A(z_R)$  are the atmospheric number densities at  $z_K$  and  $z_R$ . The atmospheric relative number density is suitably modeled by MSIS-00 [*Picone et al.*, 2002]. From equation (1) and using atmospheric number density given by MSIS-00, the unknown Rayleigh photon count  $N_R(z_K)$  in the K layer can be precisely estimated from the known Rayleigh photon count  $N_R(z_R)$  at the normalization altitude. The estimated Rayleigh count  $N_R(z_K)$  is then subtracted from the K layer data. This removes Rayleigh contamination from within the metal layer. This Rayleigh subtraction technique has been practiced by *Chu et al.* [2005], *von Zahn and Höffner* [1996], and *Höffner and Friedman* [2005], and proven to be sufficient and accurate.

[12] The current analysis also benefits from new methods of averaging and binning data. In *Friedman* [2003] mean temperature profiles were computed on a night-by-night basis by integrating photon counts. It has generally been the practice to compute a mean temperature profile for each individual observation period (e.g., one night) with a minimum number of observing hours in order to apply to the climatology [*She et al.*, 1993; *Chen et al.*, 2000; *Friedman*, 2003], sometimes by integrating photon counts and others by averaging all temperature profiles over the course of that observing period. Both of these methods produce a single mean temperature profile for each observation session, but each is problematic. The total photon count method used by *Friedman* weighs data more where there are more photons than where there are fewer. Thus, at a given altitude, if there is a sporadic layer or other short-term enhancement in the atom density during an observation, the period during this enhancement will get greater weight than other times. Computing temperature profiles for short time intervals reduces the influence of layer enhancements providing more photons (although not for the case of sporadic layers appearing above the normal layer). Additionally, when comparing one night to another, differing observation time periods can become an issue if those periods are substantially different. Thus, previous climatologies used only nights with a lot of data. For example, *Chen et al.* [2000] used only extended observations with small data gaps, and *Friedman* [2003] limited the data to nights with 5 or more hours of observations. This is difficult at sites where local weather conditions often interrupt observations, as is the case during some seasons in Arecibo. For this reason, in this work, we have adopted the method used by *Chu et al.* [2005] of building composite nights (see section 4.1 for details). This composite averaging method limits the influence of modulations and anomalies in the temperature profiles, as well as observational gaps caused by bad weather. The resulting temperature is a close representation of the mean state at each time and height within a given averaging period, which is monthly and nocturnal for this work. Even short observations are made use of in this scheme, as they contribute only to averaging with the same period of time within the composite night.

## 3. Observations

[13] The nocturnal data used in this study were collected by the Arecibo K Doppler lidar from December 2003 to

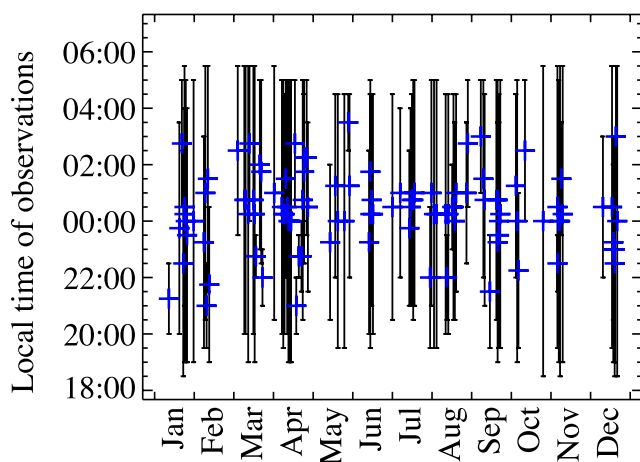


**Figure 2.** Statistics of the observational hours per night versus the day-of-year at Arecibo. These observations took place over the course of 33 months and are folded into a single year.

September 2006. Figure 2 shows the observation periods versus day number, folded into a single year. Each night is represented by a blue ‘+’ symbol with the vertical lines showing the extent of the observing period (from start to stop of data collection). The longest nights of over 11 hours are in the winter solstice period, while mid-summer nights are over 9 hours long. Across the 34 months of the data collection period there are 106 observing nights with a total of 742 hours of data, as summarized in Table 1. These data are fairly evenly distributed throughout the year, with no large gaps, and cover all 12 months. Of the 106 nights, 3 occurred in December 2003 following the system corrections discussed above, 29 during 2004, 57 in 2005, and 17 in 2006. The data distributions by month are given in Table 1, with the number of nights and hours of observing by year and the total for each month. These range from 5 nights and 33 hours in February, to 17 nights and 123 hours in April, the variability of which can be attributed to three factors: weather, equipment condition, and personnel. Other factors that affect the observations and the statistical quality of the data include attenuation from the lower atmosphere, such as clouds and haze, which are more of a problem from May to October than from November to April, and low K density, which occurs during equinox periods [Friedman *et al.*, 2002].

[14] A three-frequency technique was used to measure mesospheric K spectra in the zenith-pointing Arecibo K Doppler lidar [She and Yu, 1994; Friedman *et al.*, 2003]. The CW seed laser was locked to a Doppler-free feature of the  $D_{1a}$  line near the peak of the K fluorescence and dual two-pass acousto-optic modulators were used to shift the cw laser frequency by  $\pm 477.6$  MHz. In order to eliminate the effect of K density fluctuations on the temperature measurements, the lidar frequency was switched between three frequencies every laser pulse. The signal was integrated respectively for 1000, 500, and 500 laser pulses at the peak and two wing-frequencies at a range resolution of 150 m. An integration time of  $\sim 65$  s is required for one complete profile containing observations at all three frequencies, although integration in data processing of up to 30 minutes

is required in order to obtain accurate temperature measurements. The K signal levels vary with season and meteorological conditions from  $<5$  counts per shot to  $>30$  counts per shot for the entire K layer. The data are processed to a resolution of 30 minutes and 450 m, and are smoothed vertically with a 2 km Gaussian window. The resulting temperature errors are about 2–3 K at the peak and  $<50$  K at the edge of the K layer.

#### 4. Monthly and Annual Mean Temperatures

[15] Based on the data collection statistics shown in Section 3, our approach to derive the climatology of Arecibo MLT thermal structures is to first classify data into 12 periods to derive monthly mean temperatures, and then construct the seasonal climatology from the 12 monthly mean temperatures. This approach gives an equal weight to each month of data and generates a climatology that is a close representation of the true mean nocturnal background thermal structure. Therefore in this section we present the monthly and annual mean temperatures, and compare them with similarly derived means from the MSIS-00 model [Picone *et al.*, 2002]. In Section 5 we derive the seasonal climatology. A detailed comparison to the lidar measurements at SOR and Maui will be given in Section 6.

##### 4.1. Monthly Composite Nights and Monthly Mean Temperatures

[16] In computing the monthly mean temperature profiles, equal weighting of temperatures from different local times is a major consideration. This is because the lidar observations are limited by weather and instrument conditions, so the data from each night are not equally distributed throughout the night; that is, some nights have data early, some only late, some have on and off periods, and most contain data around local midnight. As discussed in section 2.2, the best approach to derive monthly mean temperatures is to give each local time-altitude bin the same weight. Thus, we have adopted the composite night approach used by Chu *et al.* [2005] and States and Gardner [2000a] for our analysis.

[17] The temperature data from each individual night were first binned to fixed altitude and time bins with spatial and temporal resolutions of 0.5 km and 0.5 hours, respectively. A composite night of data for each month was then

**Table 1.** Arecibo K Lidar Observing Statistics by Month From December 2003 to September 2006

Month	Total	2003		2004		2005		2006	
	Days/Hours	Days/Hours	Days/Hours	Days/Hours	Days/Hours	Days/Hours	Days/Hours	Days/Hours	Days/Hours
January	9/71			4/28					5/43
February	5/33					5/33			
March	11/72			2/8		9/64			
April	17/123			1/4		13/104		3/15	
May	6/35			2/11		2/16		2/8	
June	6/39			3/21		3/18			
July	8/56			6/41		1/7		1/8	
August	14/89			8/50		4/30		2/9	
September	11/78					7/44		4/34	
October	5/37			1/5		4/32			
November	6/47			1/2		5/45			
December	8/62	3/26		1/5		4/31			
<b>TOTAL</b>	<b>106/742</b>	<b>3/26</b>		<b>29/175</b>		<b>57/424</b>		<b>17/117</b>	

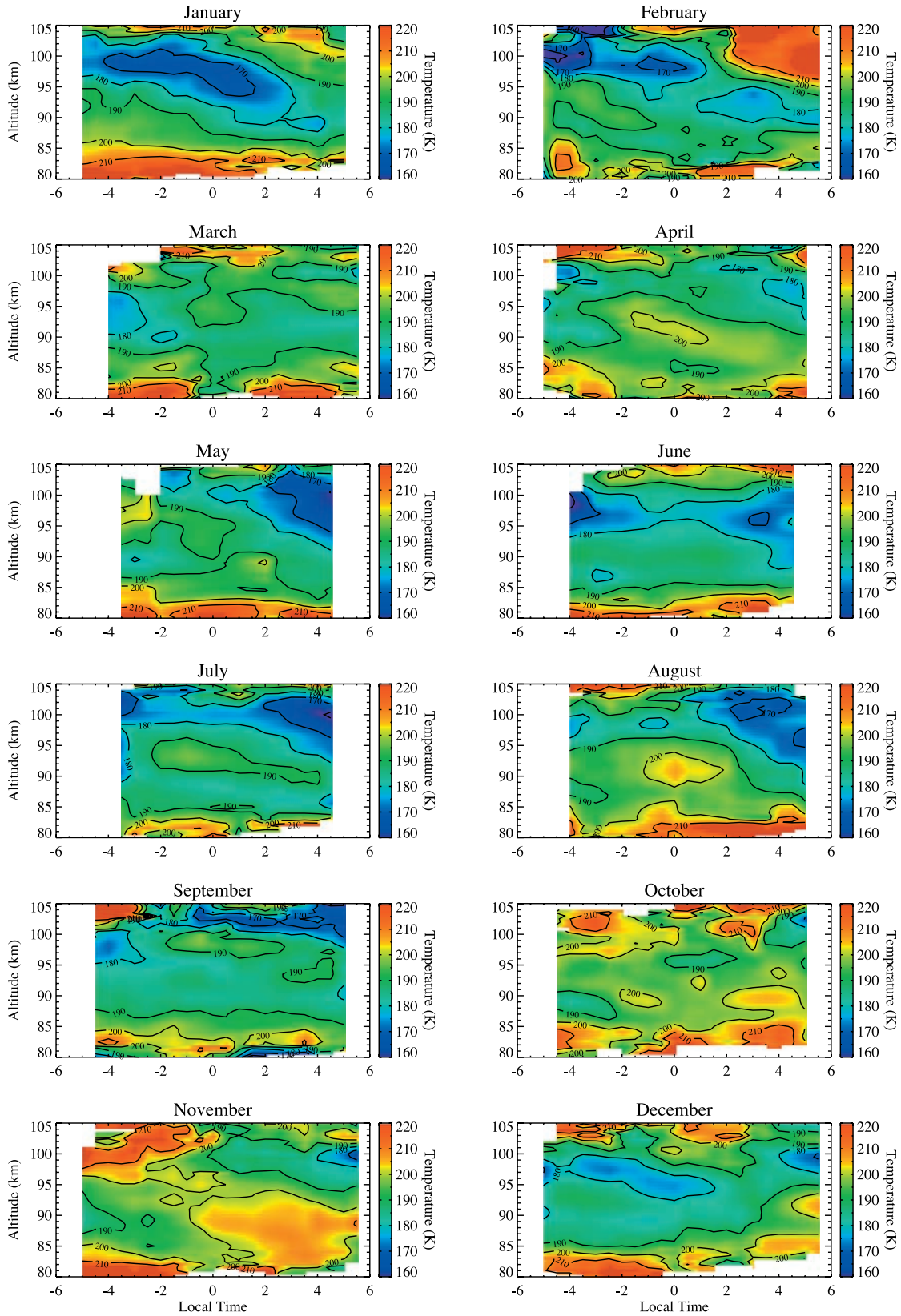


**Figure 3.** Monthly composite night temperatures for 12 months at Arecibo.

obtained by averaging the data in the same local time and altitude bins for different nights within each month. The composite night data were first spatially and then temporally smoothed using Hamming windows with full widths of 3 km

and 3 hours, respectively. The resulting monthly composite night usually covers most of the night from sunset to sunrise. Illustrated in Figure 3 are the 12 months of composite nights obtained at Arecibo. The time has been adjusted to the local



**Table 2.** Monthly and Annual Mean Temperature (K) at Arecibo

Alt (km)	Jan	Feb	Mar	Apr	May	Jun	Jul	Aug	Sep	Oct	Nov	Dec	Annual
105.0	201.1	201.3	197.2	201.8	192.8	209.5	197.2	203.4	190.5	216.0	202.7	204.4	198.4
104.0	197.1	197.7	204.9	201.5	185.6	201.0	181.7	191.3	187.8	203.7	200.3	203.6	195.6
103.0	189.7	198.8	197.0	198.5	180.2	197.1	180.0	185.5	184.3	198.3	202.0	200.9	192.0
102.0	186.9	192.1	194.6	191.0	177.5	191.2	174.1	183.0	175.8	200.3	199.9	194.5	187.9
101.0	185.1	191.0	191.8	185.7	176.6	184.5	171.5	180.8	179.4	201.9	198.7	190.9	185.9
100.0	181.2	188.6	191.0	184.4	179.1	178.7	171.2	179.1	183.1	197.6	195.9	187.7	184.1
99.0	177.4	187.5	192.3	183.9	180.9	176.6	174.4	178.2	185.9	196.3	195.1	184.5	183.6
98.0	176.7	186.8	190.7	185.4	182.6	174.8	177.9	178.2	187.2	197.5	194.0	182.1	183.6
97.0	177.3	187.8	187.8	186.0	184.6	173.8	180.9	180.0	186.1	196.1	195.6	180.9	184.1
96.0	178.7	188.1	187.3	187.3	185.9	174.9	183.1	183.2	183.9	193.2	195.8	180.9	184.8
95.0	179.6	187.2	187.5	188.5	185.8	176.8	184.7	187.0	184.2	193.0	196.1	182.3	185.9
94.0	181.0	185.4	186.4	189.6	185.8	178.9	186.1	189.7	185.3	194.9	196.7	184.0	186.9
93.0	182.3	184.4	184.8	190.7	186.5	181.5	187.9	191.6	186.1	196.2	197.8	186.3	188.0
92.0	184.1	184.3	183.9	191.6	186.7	183.9	188.8	193.3	186.1	196.8	198.8	187.4	188.8
91.0	185.4	184.9	183.6	192.4	186.4	185.5	188.1	195.0	185.3	197.4	199.1	186.6	189.2
90.0	186.4	185.4	184.3	193.2	186.8	186.2	186.6	194.3	184.7	197.5	199.0	185.5	189.3
89.0	187.1	186.7	186.7	194.5	187.9	185.3	185.4	193.0	185.5	196.9	199.4	185.7	189.6
88.0	189.0	188.7	189.4	195.2	188.5	184.2	184.9	191.9	187.5	196.1	199.5	187.9	190.2
87.0	191.7	190.4	192.0	195.5	189.7	184.0	184.6	192.7	190.1	195.8	199.3	190.2	191.2
86.0	194.4	191.3	193.5	196.0	191.9	186.1	184.8	195.0	192.4	197.7	199.6	193.3	192.9
85.0	199.2	192.3	194.8	196.6	193.3	190.4	187.2	197.1	194.8	202.6	199.9	196.3	195.3
84.0	203.8	193.7	195.4	197.7	195.0	195.1	190.9	199.1	198.8	206.3	201.5	199.8	198.0
83.0	210.9	195.5	198.3	199.9	198.5	201.2	196.8	201.7	201.8	207.9	202.7	201.9	201.4
82.0	209.5	202.3	204.8	201.3	206.1	205.4	207.6	212.4	202.4	208.4	205.7	204.4	205.7
81.0	220.8	203.9	210.3	202.1	213.5	211.3	199.8	217.4	192.7	206.0	211.1	212.3	208.3
80.0	227.8	196.1	217.0	201.6	216.4	212.6	202.7	211.5	184.8	196.9	232.7	219.3	210.5

[18] Also plotted in Figure 4 are the monthly mean temperatures derived from the MSIS-00 [Picone *et al.*, 2002] for comparison to the lidar measurements. Three mean periods were computed from the MSIS model: 1) the nighttime mean corresponding to the same 10-hour period centered about local midnight at Arecibo (green solid curves), 2) the daytime mean corresponding to the remaining 14 hours centered about local noon (blue solid curves), and 3) the 24-hour diurnal mean (red dashed curves). Apparently, the MSIS-00 model has counted in some diurnal variations, as its nighttime means are warmer than its daytime means between 80 and 103 km. In the range of 90–100 km the differences reach 10–20 K. The lidar data in the range of 85–100 km are generally colder than the MSIS nighttime means from April to September, but warmer than the MSIS in October and November. From December to March, the lidar profiles have very different shapes than the MSIS data. The lidar monthly means in Figure 4 show much more month-to-month variability than the MSIS-00 results, particularly in the profile shapes, mesopause altitudes, and mesopause temperatures. MSIS fails to predict the low mesopause altitude ( $\sim 91$  km) in spring, the mesospheric inversion layer near 90 km in summer, and the warm mesopause region in autumn. MSIS predicts a consistently high mesopause altitude, above 95 km, which the Arecibo measurements do not support.

[19] A feature shown in Figure 3 is the apparent downward phase propagation in all 12 months of composite night data. This indicates the tidal wave influence in the nocturnal temperature structure. Since the monthly composite data were obtained through averaging many nights of data in the same local time, most non-coherent waves, such as gravity waves, should have been smoothed out. The remaining wave structures are largely due to coherent waves, such as migrating solar tides synchronous with the diurnal cycle and

its harmonics. When averaging the composite nights through the 10-hour period around local midnight to derive the monthly mean temperatures, the influence of semidiurnal tides has been largely removed. A severe limitation of the nighttime-only observation window is that diurnal tides cannot be assessed, so the monthly means in Figure 4 are not independent of their influence. Lacking information on the diurnal tides, the monthly mean temperatures shown in this section represent only *the nocturnal thermal structure* at Arecibo. A full assessment of the diurnal mean background requires measurements covering the full diurnal cycle, which, once they are obtained, will prompt a reassessment of the seasonal mean mesopause state.

#### 4.2. Annual Composite Night and Annual Mean Temperature

[20] The annual composite night was obtained by averaging the monthly composite nights over 12 months in the same local time. The annual mean temperature was then derived by averaging the annual composite night over the 10-hour period centered about local midnight. The resulting annual composite and annual mean are plotted in Figures 5a and 5b. It is necessary to point out that due to the limited local-time coverage of measurements in summer (May to August), the annual composite night temperature from  $-6$  to  $-4$  LT and from  $+4.5$  to  $+6$  LT may be biased toward winter temperature. In particular, the July and August temperatures above 95 km at the end of the night are about 40 K colder than the February temperatures. The lack of summer-month temperatures from  $+4.5$  to  $+6$  LT may result in bias of 8–10 K in this region at these local times. Since the annual mean temperature is obtained by averaging the annual composite night from  $-5$  to  $+5$  LT in every 0.5-hour interval, the potential bias in the annual mean temperature is less than 1 K.

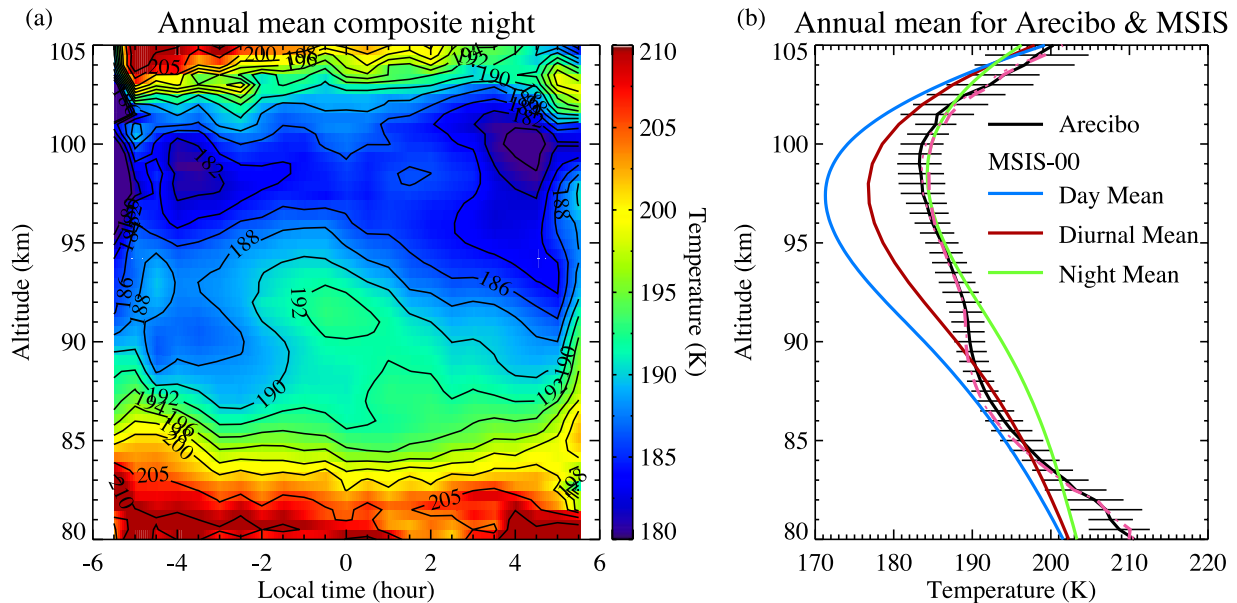


**Figure 5.** (a) Annual composite night and (b) Annual nocturnal mean temperature profile at Arecibo. Also plotted in Figure 7b are the MSIS-00 nighttime (green), daytime (blue), and diurnal (red) means through an entire year at Arecibo for comparison. The horizontal lines spanning the lidar annual mean temperature profiles indicate the geophysical variability derived from the standard deviation of the annual mean composite night shown in Figure 7a. Included in (b) are the nocturnal mean profiles using the fitted climatology mean (dashed-pink) and the average of 12 monthly means (dotted-pink).

[21] A unique feature of the Arecibo annual composite is the small temperature variation through the night at any given altitude. This can also be seen in the temperature variability plotted as the horizontal error bars spanning the annual mean profile in Figure 5b. The annual mean night geophysical variability is computed as the standard deviation of the annual composite night data at each altitude and is typically around 3 K for Arecibo. This implies that there is a very small residual semidiurnal tide in the Arecibo annual mean composite night. A downward phase propagation is still apparent between 85 and 95 km but with much smaller tidal amplitude when compared to those in annual composite night data from midlatitude SOR and subtropical Maui [Chu *et al.*, 2005]. Returning to Figure 3, a change in semidiurnal tide phase is apparent between winter and summer seasons. This results in a cancellation in the tidal oscillation and may account for the lack of a strong residual tidal signature in the annual composite night. The residual semidiurnal tides are largely removed when averaging through the composite night to derive the annual mean. However, the diurnal tidal influence may remain. Thus, we claim that our annual mean temperature profile is the nocturnal annual mean temperature profile for Arecibo.

[22] It is useful to consider the results of different approaches to derive the annual mean. Besides the mean composite night described here, there are two more methods to derive the annual mean. One is to apply a harmonic fit (a mean plus an annual and a semiannual sinusoidal variation) to the 12 monthly means and then to use the fitted mean to represent the annual mean. This is represented by the dashed pink curve in Figure 5b. Another method is to average the 12 monthly means directly to derive the annual mean, which is plotted as

a dotted pink curve in Figure 5b. Our results show that the annual means derived from all three approaches are essentially identical (<1 K differences throughout the altitude range, making the pink curves barely distinguishable). This indicates the reliability of the annual composite method and the annual mean shown in Figure 5.

[23] The Arecibo annual mean (Figure 5b) is significantly different from any other annual means measured by lidars at the high, mid, and low latitudes. One feature of the annual mean at Arecibo is the nearly flat temperature from 87 to 95 km, and even between 85 and 103 km the temperature does not depart more than  $\sim 5$  K from 189 K. This appears to be the result of a very weak temperature inversion layer in the Arecibo annual mean night between about 2200 and 0200 local time. The mesopause altitude is located at 98.5 km with a temperature of 183.6 K, which closely matches the MSIS-00 nocturnal mean. In fact, the annual nocturnal mean structure from 92 to over 102 km is almost precisely tracked by MSIS. Outside of this range the agreement is not as good, though the two mean profiles are never far apart. Between 83 and 90 km, the Arecibo profile is close to the diurnal MSIS profile, while lower down the Arecibo profile gives a hint of a temperature inversion layer near 80 km, a phenomenon frequently seen in Rayleigh lidar and rocket sonde-measured temperature profiles [e.g. Schmidlin, 1976; Meriwether *et al.*, 1998; Meriwether and Gardner, 2000].

## 5. Seasonal Climatology of MLT Temperatures

[24] The 12 monthly mean temperature profiles are shown in a color range-time-intensity (RTI) plot in Figure 6a. To construct the seasonal climatology from these 12 monthly

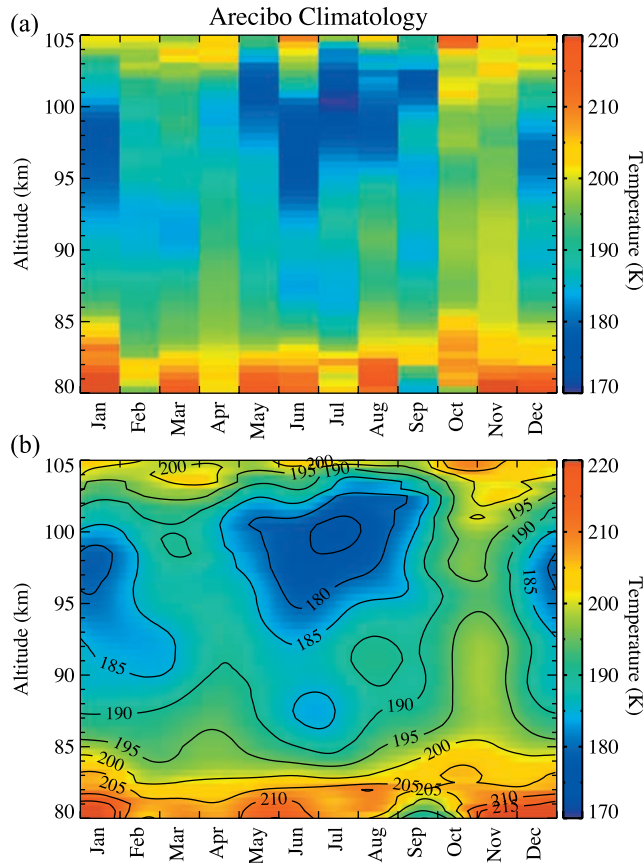


**Figure 6.** Seasonal variations of nocturnal temperature in the MLT region (80–105 km) at Arecibo. Figure 6a shows the monthly mean temperature profiles, and Figure 6b shows the climatology after standard processing detailed in the text.

mean temperature profiles we applied a harmonic fit given by equation (2):

$$T(z, t) = T_0(z) + A_{12}(z) \cos \left[ \frac{2\pi}{365} (t - \Phi_{12}(z)) \right] + A_6(z) \cos \left[ \frac{2\pi}{365/2} (t - \Phi_6(z)) \right] \quad (2)$$

where  $T(z, t)$  is the temperature at date  $t$ , expressed in day of the year (1–365), and altitude  $z$ ,  $T_0(z)$  is the background mean temperature at  $z$  (the dashed pink curve in Figure 5b),  $A_{12}(z)$  and  $\Phi_{12}(z)$  are, respectively, the amplitude and phase of the annual variation, and  $A_6(z)$  and  $\Phi_6(z)$  are the amplitude and phase of the semi-annual variation. The fitted temperature  $T(z, t)$ , i.e., the mean plus the annual and semiannual harmonic fits, was subtracted from the raw monthly means and the residuals were smoothed using a Hamming window with a FWHM of 6 weeks and a time resolution of 1 day. The smoothed residual temperature (with 1-day resolution) was then added back to  $T(z, t)$  (i.e., the mean plus annual and semiannual harmonic fits). The resulting seasonal climatology of the MLT temperature at Arecibo is plotted in Figure 6b. The amplitudes ( $A_{12}$  and  $A_6$ ) and phases ( $\Phi_{12}$  and  $\Phi_6$ ) of corresponding annual and semiannual fits are shown in Figure 7.

[25] There is a clear signature of semiannual variations in this tropical seasonal climatology, in stark contrast to mid- and high-latitude sites, e.g., SOR, Urbana, Fort Collins, and South Pole, where annual variations dominate the seasonal temperature climatology [Chu *et al.*, 2005; States and Gardner, 2000a; Chen *et al.*, 2000; Pan and Gardner, 2003]. This appears to be mainly caused by the decreasing annual amplitude at Arecibo, rather than the increasing semiannual amplitude. While the annual amplitude  $A_{12}$  is much larger than the semiannual amplitude  $A_6$  at mid and high latitudes,  $A_{12}$  and  $A_6$  have similar amplitudes in the Arecibo seasonal climatology. The Arecibo semiannual amplitude  $A_6$  is comparable or slightly larger than that at mid and high latitudes. At Arecibo,  $A_6$  increases with altitude from a low of 1 K near 82 km and reaches  $\sim 7.5$  K around 98 km, dropping again above that altitude. Meanwhile,  $A_{12}$  is under 2 K near the bottom of the layer, oscillates about  $3.3 \pm 1$  K until 96 km where it increases rapidly to over 8 K around 100 km. These compare well with the amplitudes derived from MSIS-00 data (shown as dotted curves in Figure 7). The lidar semiannual amplitude has sharper features than the model predictions, but they are essentially similar. The MSIS annual amplitude has a node near 92 km, which is not seen in the lidar amplitude, but otherwise the similarity is remarkable. As for the phases, the lidar observed semiannual phase ( $\Phi_6$ ) is quite constant with altitude near day 110 from 84 to 104 km, which is similar to, though somewhat later than, the MSIS-00 model prediction. The lidar annual phase ( $\Phi_{12}$ ) peaks around day 300 near the low extreme, gradually increasing with altitude until, at the top of the layer, it rolls over to the beginning of the year. The MSIS annual phase is close to the observed results below 87 km but almost opposite to the observed annual phase above 90 km.

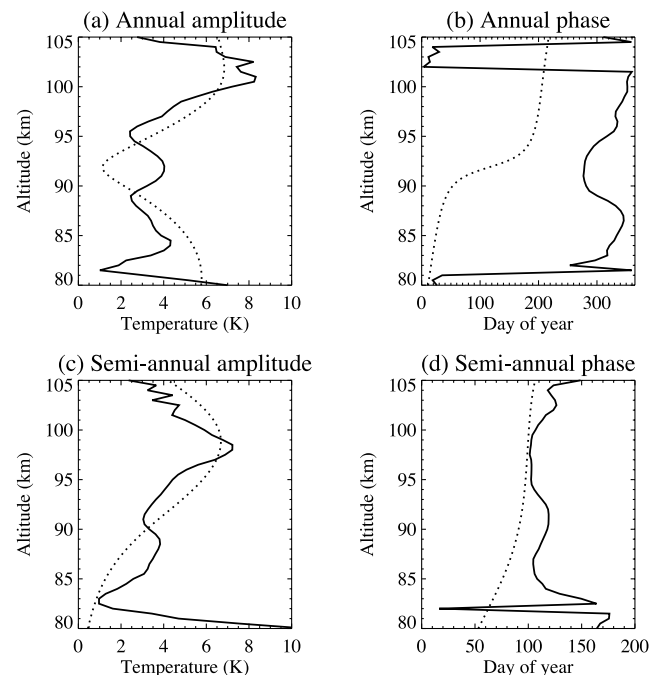


**Figure 7.** Comparison of annual and semiannual amplitudes and phases between the Arecibo lidar data (solid curves) and the MSIS-00 model (dotted curves).

[26] Figure 6 exhibits a few unique characteristics of the Arecibo MLT temperature structure. This seasonal climatology shows a high mesopause altitude ( $\sim 100$  km) in summer, a medium mesopause altitude ( $\sim 96$  km) in late autumn and winter, and a low mesopause altitude around the spring equinox ( $\sim 91$  km). This is completely different from what has been observed at mid and high latitudes, or even subtropical latitudes, where the mesopause shows a winter high altitude ( $\sim 101$  km) and a summer low altitude ( $\sim 87$  km) [Chu *et al.*, 2005; States and Gardner, 2000a; She *et al.*, 2000; Pan *et al.*, 2002; Pan and Gardner, 2003; Kawahara *et al.*, 2004]. In addition, the Arecibo climatology shows warmer mesopause temperatures around the equinoxes with the autumnal equinox being warmest. We would like to point out that the sampling in October is less than for most other months. However, although future October observations at Arecibo are required to confirm whether the 2005 October state is indicative of the mean, the fact that November is also warm, with more years of observations, is compelling. The observed mesopause temperature is cold in both winter and summer, although summer is  $\sim 5$  K colder than winter. This is also very different from the mid and high latitudes where the mesopause temperature is much colder in summer than in winter. It is also different from observations in Maui, where January and July mesopause temperatures are both about 16 K warmer than those for Arecibo [Chu *et al.*, 2005].

[27] To illustrate the variations in the Arecibo mesopause more clearly, the Arecibo mesopause was determined for every single day throughout the year from the seasonal climatology shown in Figure 6b, and the resulting mesopause altitude and mesopause temperature are plotted as the solid curves in Figure 8. Deriving the mesopause from a smoothed climatology has a major advantage over the mesopause determined from individual nights of data, because the seasonal climatology in Figure 6b is sufficiently averaged over many hours of data that most of the wave effects are smoothed out. Thus, the mesopause characteristics shown in Figure 8 reflect those of the mean background temperature, rather than the individual nights that are heavily affected by day-to-day wave activity. The three-level mesopause altitude, the warm equinox mesopause temperatures, and the cold winter and summer mesopause temperatures described above are clearly delineated in Figure 8. These features are different from both lidar measurements at other locations and from MSIS-00. The mesopause determined from MSIS-00 data is shown as the dashed curves in Figure 8. It has very small seasonal variations in altitude, from a peak of  $\sim 100$  km in spring to a minimum near 96 km in autumn, and the temperatures are colder than the lidar observations in winter, warmer in summer, and the equinox maxima, though similar in temperature, occur later in spring and earlier in autumn than those measured.

## 6. Comparison of Arecibo With SOR and Maui

[28] Many unique and interesting features emerge from this first complete range-resolved seasonal climatology of the mesopause region at a tropical latitude. The seasonal temperatures show very different variability than the climatology obtained at mid latitudes. In light of the recent

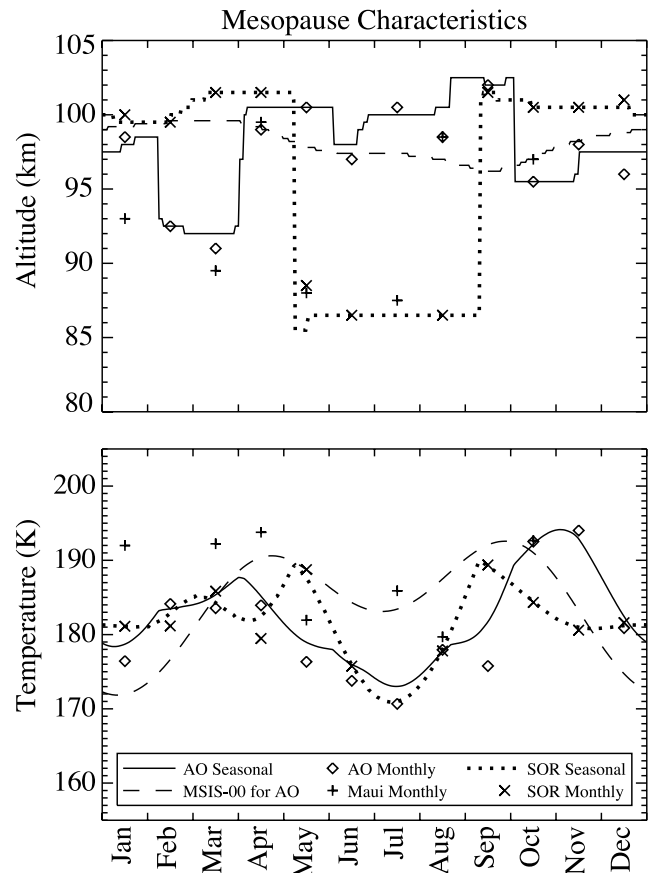


**Figure 8.** Seasonal variations of the nocturnal mesopause altitude and temperature at Arecibo (solid line and diamonds), coupled with those for SOR (dotted line and 'x' symbols), Maui ('+' symbols), and the MSIS-00 nocturnal values for Arecibo (dashed line).

publications of MLT thermal structures at SOR by the University of Illinois Na wind and temperature lidar [Chu *et al.*, 2005] and at Maui by the same Na lidar [Chu *et al.*, 2005], it is of great value to make a detailed comparison relating the climatologies of these sites. The purpose of this comparison is to characterize the seasonal similarities and differences in temperature structures between the tropical site Arecibo ( $18.35^{\circ}\text{N}$ ), the sub-tropical site Maui ( $20.7^{\circ}\text{N}$ ), and the midlatitude site SOR ( $35^{\circ}\text{N}$ ) through the MLT region.

### 6.1. Mesospheric Temperature Inversion Layers

[29] The comparisons of monthly and annual means among Arecibo, Maui, and SOR are given in Figures 9 and 10. An obvious difference is the much weaker (nearly non-existent) mesospheric temperature inversion layers (MTIL) near 90 km in the Arecibo annual mean when compared to Maui and SOR annual means. Seasonally the Arecibo MTILs are very weak from October to April but have considerable amplitude from May to September. MTILs are a prominent feature in the nocturnal MLT region at mid latitudes as reviewed by Meriwether and Gardner [2000] and observed by Na Doppler lidars at Fort Collins ( $41^{\circ}\text{N}$ ), Urbana ( $40^{\circ}\text{N}$ ), and SOR ( $35^{\circ}\text{N}$ ) [Chen *et al.*, 2000; States and Gardner, 2000b; Chu *et al.*, 2005]. Chu *et al.*

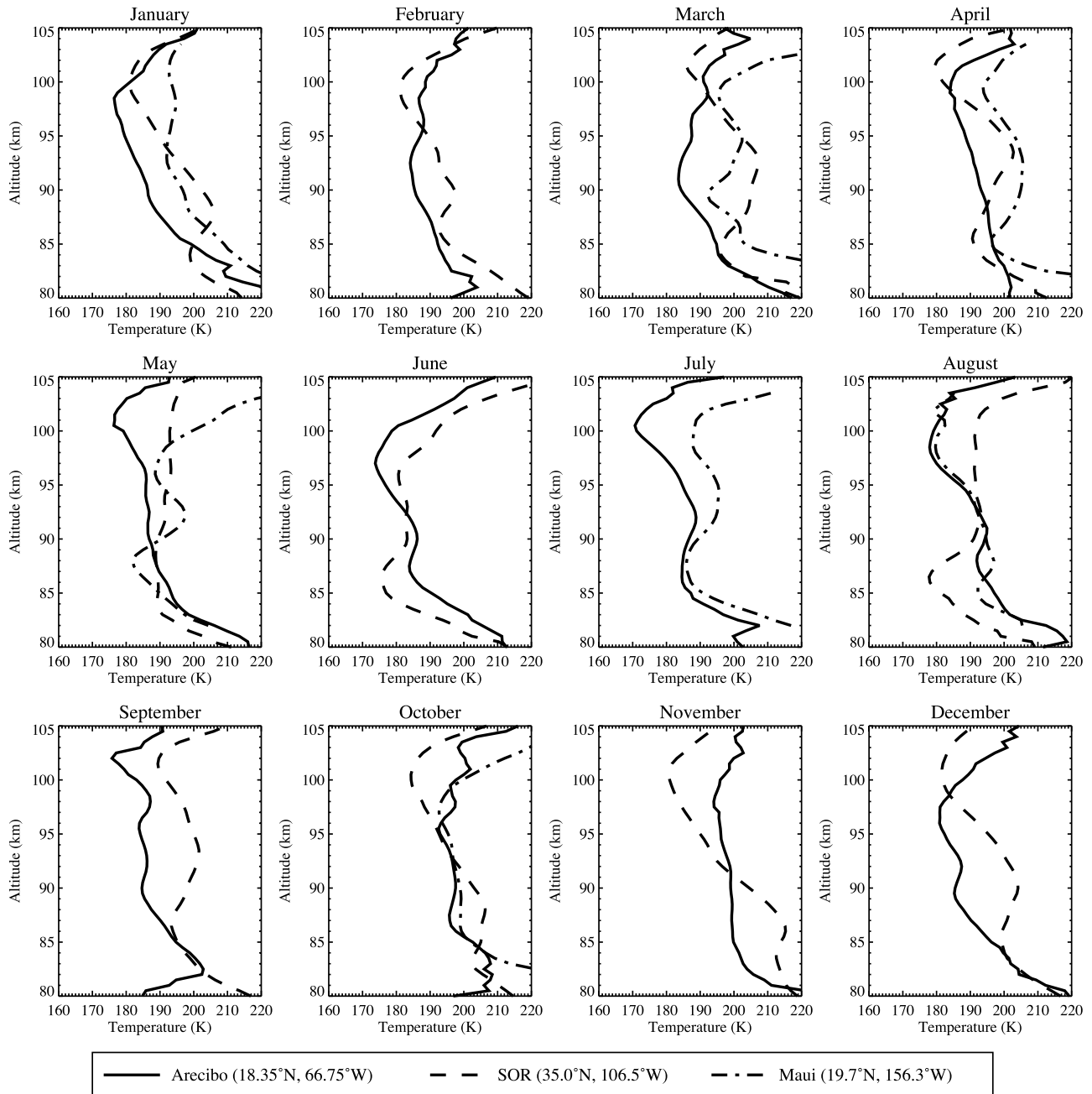


**Figure 9.** Comparison of nocturnal monthly mean temperatures among Arcibo, SOR, and Maui. The Arcibo monthly means (same as shown in Figure 4) are shown as the solid curves. SOR monthly means (11 months with July missing) are illustrated as the dashed curves, and Maui monthly means (7 months) are plotted as the dot-dashed curves. The temperature errors and variability for SOR and Maui can be found in *Chu et al.* [2005].

[2005] presented the characteristics of the nocturnal MTIL near 90 km and found that the amplitude was generally much stronger at mid latitude SOR than at the sub-tropical site Maui. This latitudinal trend is reaffirmed by our observations at Arcibo, as the MTIL amplitude experiences a further decrease from sub-tropical Maui to tropical Arcibo. Table 3 reproduces Table 5 from *Chu et al.* [2005] with the addition of 3 months (March, May, August) at Maui and 12 months at Arcibo. In all months where comparisons can be made (11 for SOR and 7 for Maui) the Arcibo MTILs are much

weaker than SOR from October to April but become comparable to SOR from May to September. The Arcibo amplitude is similar to Maui in January, July, August, and October but much weaker than Maui during the spring equinox (March to May).

## 6.2. Mesopause Characteristics

[30] As described in Section 5, we observe a 3-level mesopause altitude at Arcibo. This is clearly shown as the solid line in Figure 8a: a high altitude ( $\sim 100$  km) from

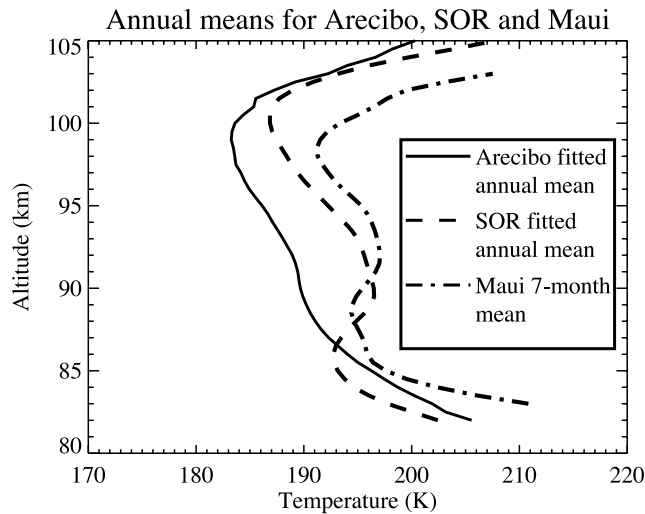


**Figure 10.** Comparison of annual mean temperatures among Arecibo (solid), SOR (dashed), and Maui (dot-dash). The SOR plot is from *Chu et al.* [2005], while the Maui profile is the 7-month mean. The temperature errors and variability for SOR and Maui can be found in *Chu et al.* [2005].

April to September, a middle altitude (~96 km) from October to January, and a low altitude (~91 km) in February and March. This is in strong contrast to the 2-level mesopause observed at midlatitude SOR, reproduced from *Chu et al.* [2005] and shown as the dotted line in Figure 8a. The SOR mesopause stays around 86.5 km from May to mid September with abrupt transitions from and to ~101 km in early May and mid September. Unlike Arecibo, no mesopause was observed in between these two altitudes. This 2-level mesopause feature is in accord with Na lidar observations at other midlatitude sites like Fort Collins (41°N), Urbana (40°N), and Tenerife (28°N). Earlier lidar observations led us to expect a 2-level mesopause in mid and high latitudes, which would collapse to the single high-level year-round mesopause in the tropics [*von Zahn et al.*, 1996; *She and von Zahn*, 1998]. Looking at the equinox period for Arecibo and Maui, it now seems that the two-

level structure may be too simplistic. While the Maui summer mesopause is at 87 km, similar to SOR, the Maui mesopause in January and March around 91 km and in October at 97 km concur with the low and middle levels observed at Arecibo. This comparison indicates that the tropical and sub-tropical regions have more than two mesopause altitudes.

[31] As for the comparison of mesopause temperatures, Arecibo and SOR have similar seasonal variations in the sense that mesopause temperatures are warmer around equinoxes and colder near solstices. However, the Arecibo mesopause is a few K warmer than SOR at summer solstice and a few K colder than SOR around winter solstice. Thus, the winter and summer mesopause difference at Arecibo (~5 K) is smaller than the difference at SOR (~10 K). While SOR spring and autumn equinoxes have similar mesopause temperatures (~190 K), the Arecibo autumn equinox (~195 K) is much warmer than the spring equinox (~185 K). Compared to SOR, the maxima of Arecibo mesopause temperature come earlier in spring and later in autumn. The Maui mesopause temperature is in general warmer than Arecibo, except in August and October when Maui and Arecibo have comparable mesopause temperatures.

[32] Plotted in Figure 11a are the seasonal variations of the Arecibo nocturnal temperatures at 86.5, 91, 96, and 100 km. The four altitudes were chosen for the low summer mesopause altitude at SOR (86.5 km) and for the three levels of Arecibo mesopause altitude (91, 96, and 100 km), of which the 100 km level is also close to the high mesopause altitude occurring in winter at SOR (~101 km). Upper and lower temperature minima at 101 and 86.5 km shown in Figure 14 of *Chu et al.* [2005] are reproduced in Figure 11b for comparison purposes. Figure 11a shows that the Arecibo temperature at 86.5 km does not fall below the minimum of other three temperatures at any time during the year. Thus, it is clear that the 86.5 km never becomes a mesopause location at Arecibo, contrary to the situations at SOR and other midlatitude sites like Fort Collins (41°N), Urbana (40°N), and Tenerife (28°N) where the summer mesopause is located around 86.5 km [*e.g. Chu et al.*, 2005; *She et al.*, 2000; *Chen et al.*, 2000; *States and Gardner*,

**Table 3.** Characteristics of the Mesospheric Temperature Inversion Layers (MTIL) at Tropical Arecibo and Comparison to mid-Latitude SOR and sub-Tropical Maui

	Jan	Feb	Mar	April	May	June	July	Aug	Sept	Oct	Nov	Dec	Mean ± Std. Dev.
<i>Altitude, km</i>													
Arecibo	90.5	87 <sup>a</sup>	86.5 <sup>a</sup>	89.0	96.5	90.5	92.5	91.0	98.5	91.0	91.5	92.0	91.4 ± 3.4
SOR	88.5	90	93	93.5	92	90	–	90.5	93.5	88.5	87	91	90.7 ± 2.2
Maui	98	–	94.5	92.5	92	–	94.5	88.0	–	90	–	–	92.8 ± 3.3
<i>Amplitude, K</i>													
Arecibo	0.8	1.0 <sup>a</sup>	1.8 <sup>a</sup>	1.5	5.2	5.6	9.9	7.5	8.6	3.0	2.0	4.3	4.3 ± 3.1
SOR	11.6	7.6	16.3	17.7	1.5	5.7	–	9.7	10.0	9.4	7.7	10.7	9.8 ± 4.5
Maui	2.2	–	8.4	10.6	12.2	–	8.5	7.5	–	2.0	–	–	7.3 ± 3.9
<i>Width, km</i>													
Arecibo	8.0	6.0 <sup>a</sup>	6.0 <sup>a</sup>	14.5	12.5	10.0	14.5	11.0	13.0	8.5	12.0	7.0	10.3 ± 3.1
SOR	16	13	17.5	16	10	9.5	–	13	14.5	17.5	16.5	15.5	14.5 ± 2.8
Maui	8	–	9.5	14.5	8	–	11.5	13.5	–	10.5	–	–	10.8 ± 2.5

<sup>a</sup>The mean temperature profiles for Arecibo in February and March show no significant MTIL. The numbers quoted here reflect the residual upon subtracting the line between temperatures at roughly 83 and 91 km.

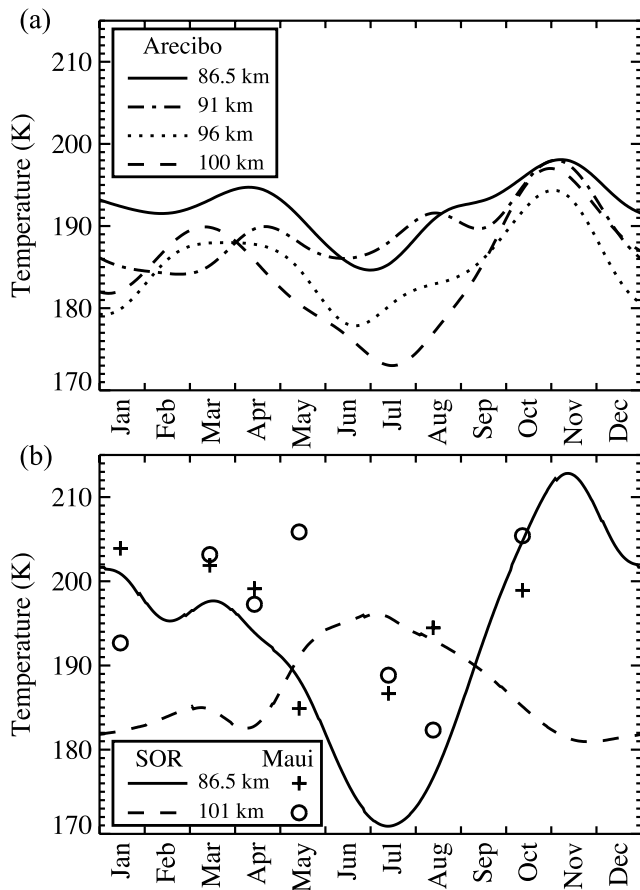


**Figure 11.** (a) Seasonal variations of the nocturnal temperatures at 86.5, 91, 96, and 100 km for Arecibo and (b) at 86.5 and 101 km for SOR and Maui. The SOR plot is reproduced from *Chu et al.* [2005]. Maui values are plotted as symbols, '+' for 86.5 km and 'o' for 101 km.

2000a; *Fricke-Begemann et al.*, 2002]. The seven months of Maui monthly mean temperatures are indicated in Figure 11b for 86.5 km and 101 km. Although Maui is only about 2.4° north of Arecibo, it exhibits a low mesopause altitude (87 km) in summer [*Chu et al.*, 2005], as is seen in Figure 11b, where the 86.5-km temperatures are colder than the 101 km temperatures in May and July. On this point, Maui is quite different from the tropical site Arecibo and similar to midlatitude sites. This is in spite of the fact that: (1) Maui exhibits two intermediate mesopause altitudes near 97 and 91 km that are similar to Arecibo but different from SOR; and (2) Maui MTIL amplitudes are close to Arecibo in some months (January, July, August, and October) and then different from Arecibo but closer to SOR in other months (March and April). This leads us to see Maui as a sub-tropical site where the MLT thermal structure is unlike that for either tropical Arecibo or midlatitude SOR, but, sharing characteristics of both, something in between.

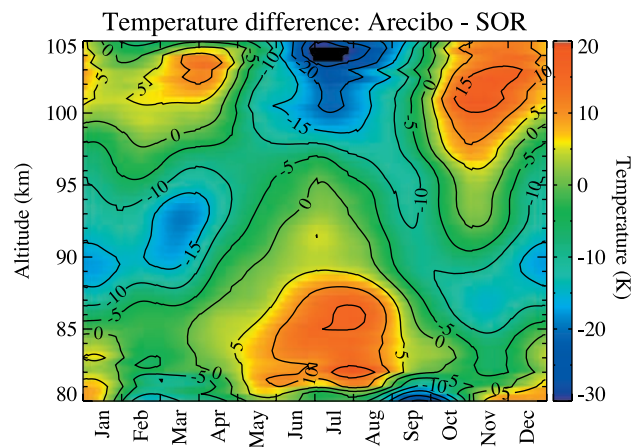
**6.3. Summer Cooling in Lower Thermosphere Temperature at Arecibo**

[33] A distinct feature between the Arecibo and SOR seasonal climatologies is that the Arecibo temperature at

100 km decreases in summer to become the seasonal minimum, while the SOR temperature at 101 km (as well as 100 km) increases in summer and becomes the maximum. This is clearly shown in Figure 6b of this paper and Figure 11 in *Chu et al.* [2005]. To further compare Arecibo with SOR, the seasonal temperature differences between Arecibo and SOR were derived by subtracting the SOR climatology (Figure 11 in *Chu et al.* [2005]) from the Arecibo climatology (Figure 6b). The resulting differences are plotted in Figure 12 as a function of season and altitude. There are three principal conclusions from this plot: 1) the Arecibo temperatures are colder than SOR in summer but warmer than SOR around equinoxes above 100 km; 2) Arecibo temperatures are colder than SOR in winter from 87 to 97 km; and 3) Arecibo temperatures are warmer than SOR in summer around 85 km.

[34] To quantitatively describe the seasonal variations in the lower thermosphere around 100 km, let us refer to Figure 11 of this paper. For Arecibo temperature at 100 km, it is 185 K at midwinter, 190 K at spring equinox, 173 K at midsummer, and 195 K in late autumn. Thus, the observed temperature change from equinoxes to summer in the nocturnal mean is ~17–22 K cooling in summer at tropical Arecibo. For SOR temperature at 101 km, it is 182 K at midwinter, 185 K at spring equinox, 197 K at midsummer, and 181 K in late autumn. Thus, the observed temperature change from equinoxes to summer in the nocturnal mean is ~12–16 K heating in summer at midlatitude SOR.

[35] It is necessary to assess the potential aliasing in the observed seasonal variations caused by under sampling of diurnal tides since the lidar observations were nighttime-only at both Arecibo and SOR. The idea behind this is that under sampling of diurnal tides may bias temperature measurements depending on the tidal phase. If the local midnight is in the crest or trough of the diurnal tides, their under-sampling may bias the measured temperature toward warmer or cooler values, respectively. If the local midnight is at a node point of the diurnal tides, under sampling of diurnal tides may not affect the measured temperature as the nocturnal average will cancel out diurnal tidal influences.



Since diurnal tidal amplitude and phase may undergo seasonal variations through the year, the bias caused by the under sampling of diurnal tides in nighttime-only observations may also vary with season, so it could contribute to observed seasonal variations.

[36] We estimate the aliasing caused by diurnal tides at Arecibo with assistance of the diurnal tidal amplitude and phase information inferred from SABER data [Zhang *et al.*, 2006]. For Arecibo temperature at 100 km, the migrating diurnal tidal phase is  $\sim 12$  hours throughout the year, meaning that local midnight is in the trough and the bias is toward colder temperatures. The migrating diurnal tidal amplitude is about 4 K at equinox and 8 K in July, so the bias from nighttime observations is about  $-2.5$  K at equinox and  $-5$  K at midsummer. From this, the temperature difference between summer and equinox caused by the seasonal variations of the bias in the case of migrating tides is estimated to be  $(-5 \text{ K}) - (-2.5 \text{ K}) = -2.5 \text{ K}$ , i.e., 2.5 K cooler in summer. For nonmigrating tides, the  $S = -3$  mode has the largest amplitude at Arecibo, while other nonmigrating tidal influences are negligible for this latitude. At 100 km, the  $S = -3$  nonmigrating diurnal tide has phase of  $\sim 12$  hours in July and  $\sim 0$  hour at equinox with amplitude of  $\sim 4$  K for both seasons. Thus, local midnight is in its crest at equinox, resulting in  $+2.5$  K bias, while it is in its trough at midsummer resulting in a  $-2.5$  K bias. The summer-to-equinox temperature difference caused by the bias variations in the case of nonmigrating diurnal tides is  $(-2.5 \text{ K}) - (+2.5 \text{ K}) = -5 \text{ K}$ . Thus, the overall aliasing caused by the migrating and nonmigrating diurnal tides is  $(-2.5 \text{ K}) + (-5 \text{ K}) = -7.5 \text{ K}$ . In other words, the pertinent components of the diurnal tide decrease the 100 km temperature at Arecibo by 7.5 K in summer as compared with equinox. Our nighttime lidar observations show the summer cooling is between 17 and 22 K. Subtracting the diurnal tidal aliasing, the actual decrease in summer lower thermosphere temperature is estimated to be  $\sim 10$  K. It is necessary to point out that the diurnal tidal amplitudes have the largest gradient near  $20^\circ$  latitude and 100 km altitude [Zhang *et al.*, 2006], which will cause relatively large uncertainty in the estimation of diurnal tidal amplitudes at Arecibo. This produces uncertainty in the estimation of the diurnal tidal aliasing. If we double the estimated aliasing to 15 K, then the summer cooling in the diurnal mean background at 100 km could be as small as 2 K above Arecibo. To fully resolve the diurnal tidal aliasing requires Arecibo lidar observations covering the full diurnal cycle.

[37] Lidar observations with full diurnal coverage are available from several midlatitude sites: Fort Collins ( $41^\circ\text{N}$ ), Urbana ( $40^\circ\text{N}$ ), and Tenerife ( $28^\circ\text{N}$ ) [She *et al.*, 2000; Chen *et al.*, 2000; States and Gardner, 2000a; Fricke-Begemann *et al.*, 2002]. These diurnal means also show the increasing temperatures in summer in the lower thermosphere ( $\sim 100$  km and above), ranging from 8–16 K, similar to the SOR nocturnal heating rate in summer. Thus, the summer warming in the lower thermosphere is a general feature at mid latitudes. As for sub-tropical sites, though only 4 months of nocturnal data were reported, the temperature in the lower thermosphere around 100 km decreased in summer [Chu *et al.*, 2005]. Now with 7 months of data gathered, the Maui MLT thermal structure exhibits a more pronounced decrease in summer in the lower thermosphere, similar to the situation at Arecibo.

The 7 months of Maui temperature at 101 and 86.5 km are plotted as circles and crosses in Figure 11b. This figure clearly shows the warm equinox and cool summer temperatures at 101 km for Maui. Thus, the summer cooling in the lower thermosphere is most likely a general feature in tropical and sub-tropical regions. We therefore conclude that the opposite seasonal variations in the lower thermosphere temperature (around 100 km) between Arecibo and SOR are representative of the difference between the tropical and midlatitude regions.

[38] The observed differences between the tropical and mid latitude sites indicate an increasing prominence of semiannual oscillation (SAO) over that of the annual oscillation (AO) in the MLT temperature structure when going from mid latitudes to tropical regions. This is particularly prominent in the lower thermosphere (100 km), where the increasing temperature in summer at mid latitudes is mainly due to increasing radiative heating caused by  $\text{O}_2$  absorption of solar far-UV radiation when going from winter to summer [Andrews *et al.*, 1987]. The increase of solar heating from winter to summer is less significant in tropical regions than at mid latitudes, thus, a tropical site like Arecibo has a smaller annual oscillation amplitude as observed. Even so, there is still increasing radiative heating in the lower thermosphere in summer in tropical regions. In order to reproduce the observed summer cooling at Arecibo, there must be some cooling mechanisms that override the radiative heating effect in the lower thermosphere. Dynamic heating and cooling associated with the semiannual oscillation (SAO) is likely a mechanism responsible for the observed results [Groves, 1972; Garcia *et al.*, 1997; Sassi and Garcia, 1997]. SAO has been observed in mesospheric temperatures by both groundbased and satellite-borne instruments [Taylor *et al.*, 2005; Takahashi *et al.*, 1995; Clancy and Rusch, 1989; Shepherd *et al.*, 2004, 2006]. However, observations in lower thermosphere temperature are still very rare. The lidar observations from Arecibo presented here provide one of the very few observations of SAO in lower thermosphere temperature. Further discussion of the SAO as a mechanism in the observed cooling is beyond the scope of this paper.

## 7. Conclusions

[39] A complete range-resolved seasonal climatology of the nocturnal thermal structure in the MLT region (80–105 km) is characterized for the first time at a tropical site using Arecibo K Doppler lidar observations. The K Doppler lidar data, covering 33 months from December 2003 to September 2006, were obtained after major improvements of the lidar instrument had been completed. Combining the improvements in lidar instrumentation with the improvements in data processing and analysis techniques, the K Doppler lidar has been proven to have high fidelity in producing accurate and precise temperature measurements in the MLT region. Using the approach of building monthly composite nights, monthly mean temperatures throughout the year were derived from 106 nights (742 hours) of K lidar data at Arecibo. Then, by applying a harmonic fit method to the 12 monthly means, the seasonal climatology of the MLT temperature was constructed for Arecibo with equal weight for each month and at each local time and

altitude. Thus, this climatology is a close representation of the nocturnal thermal structure of the Arecibo MLT region.

[40] Several unique features are shown in the Arecibo seasonal climatology that are very different from mid and high latitude observations. First, the mesospheric temperature inversion layers are only significant in summer at Arecibo and they are virtually non-existent during the rest of the year, while the MTILs are nearly a persistent feature in the nocturnal MLT region at mid latitudes, though they are weaker in summer than during other seasons. Second, the low mesopause altitude around 86.5 km at mid latitudes never occurs in the Arecibo MLT region. Instead, the Arecibo climatology shows a three-level mesopause altitude with the high altitude in summer ( $\sim 100$  km), the medium altitude in late autumn and winter ( $\sim 96$  km), and the low altitude in early spring ( $\sim 91$  km). Third, Arecibo has similarly cold mesopause temperatures in both winter and summer, with summer ( $\sim 171$  K) only marginally colder than winter ( $\sim 176$  K), which is contrary to the mid and high latitudes where the summer mesopause is much colder (10–60 K) than the winter mesopause. The mesopause temperature is warm around equinoxes with the warmest in autumnal equinox at Arecibo. Fourth, Arecibo exhibits warm temperatures throughout the MLT region at equinoxes, particularly following the autumnal equinox. The warm autumnal equinox phenomenon is similar to the mid latitude observations at SOR and Urbana. Fifth, the lower thermosphere around 100 km at Arecibo shows a decreasing temperature in summer (when it reaches its coldest temperature). This summer cooling in lower thermosphere is contrary to the increasing temperature in summer observed at all mid latitude locations. And sixth, in most of the altitude range from 80–105 km, the Arecibo seasonal variations are dominated by both semiannual and annual variations, rather than by the annual variations as observed at mid latitudes. This is principally due to a decreasing annual amplitude toward lower latitudes, rather than an increase in the semiannual amplitude. In the semiannual oscillation observed over Arecibo the autumn equinox is warmer than the spring equinox, which is contrary to airglow observations at low latitude sites where the mesospheric semi-annual oscillation has been studied [Taylor *et al.*, 2005].

[41] The observed opposing seasonal variations in the lower thermosphere temperatures around 100 km between the tropical sites and the midlatitude sites is likely related to the observed increasing importance of semiannual oscillation when going from the mid latitudes to the tropical regions. However, it is unclear to us whether the SAO is the cause or effect of the summer cooling in the lower thermosphere temperature. The SAO of temperature in the mesopause region, especially in the lower thermosphere, is still a little understood phenomenon. This requires further investigation through improved observations, modeling, and theory.

[42] Finally, it is exceedingly clear that lacking knowledge of the diurnal tide, due to nighttime-only measurements, limits the possibilities of further interpretation of many observed phenomena. Thus, many of the features of the mesopause region over Arecibo cannot be completely understood. The SAO and the lower thermosphere summer

cooling, MTILs and their seasonal variations, and the mesopause temperature are all features of the tropical MLT that require full-diurnal-coverage observations. For this reason, lidar observations at sites such as Arecibo,  $\sim 20^\circ$  latitude where diurnal tidal amplitudes have very large gradients, need to be made during daylight hours. The necessary upgrade to the lidar for full-diurnal-coverage operations is underway at Arecibo.

[43] **Acknowledgments.** The Arecibo Observatory is operated by Cornell University under a cooperative agreement with the National Science Foundation. This work is also supported by NSF CEDAR grant ATM-05-35457. XC is supported by NSF Grants ATM-06-02334 and ATM-06-32501. The authors thank Mr. Rubén Delgado for his tireless help with observations. We also thank Dr. Hanli Liu, Dr. Jeffrey Forbes, and Ms. Xiaoli Zhang for valuable discussions. We appreciate Dr. Jeffrey Forbes and Ms. Xiaoli Zhang for providing us the analysis results of SABER tidal data. XC wishes to acknowledge the generous assistance of Dr. Sixto González and Cornell University through Award 49759-8180, which supported her role in this project. The authors greatly appreciate the diligent work of the reviewers of this paper, whose contributions, though anonymous, were significant.

## References

- Andrews, D. G., J. R. Holton, and C. B. Leovy (1987), *Middle Atmosphere Dynamics*, 489 pp., Academic Press, San Diego.
- Arnold, K. S., and C. Y. She (2003), Metal fluorescence lidar (light detection and ranging) and the middle atmosphere, *Contemp. Phys.*, *44*(1), 35–49.
- Chen, S., Z. Hu, M. A. White, H. Chen, D. A. Krueger, and C. Y. She (2000), Lidar observations of seasonal variation of diurnal mean temperature in the mesopause region over Fort Collins, Colorado ( $41^\circ\text{N}$ ,  $105^\circ\text{W}$ ), *J. Geophys. Res.*, *105*(D10), 12,371–12,379.
- Chu, X., and G. C. Papen (2005), Resonance Fluorescence Lidar for Measurements of the Middle and Upper Atmosphere, in *Laser Remote Sensing*, edited by T. Fujii and T. Fukuchi, pp. 179–432, CRC Press, Taylor & Francis Group.
- Chu, X., C. S. Gardner, and S. J. Franke (2005), Nocturnal thermal structure of the mesosphere and lower thermosphere region at Maui, Hawaii ( $20.7^\circ\text{N}$ ), and Starfire Optical Range, New Mexico ( $35^\circ\text{N}$ ), *J. Geophys. Res.*, *110*, D09S03, doi:10.1029/2004JD004891.
- Clancy, R. T., and D. W. Rusch (1989), Climatology and trends of mesospheric (55–90 km) temperatures based upon 1982–1986 SME limb scattering profiles, *J. Geophys. Res.*, *94*, 3377–3393.
- Clemesha, B. R., I. Veselovskii, P. P. Batista, M. P. P. M. Jorge, and D. M. Simonich (1999), First mesopause temperature profiles from a fixed southern hemisphere site, *Geophys. Res. Lett.*, *26*(12), 1681–1684.
- Fricke-Begemann, C., J. Höffner, and U. von Zahn (2002), The potassium density and temperature structure in the mesopause region (80–105 km) at a low latitude ( $28^\circ\text{N}$ ), *Geophys. Res. Lett.*, *29*(22), 2067, doi:10.1029/2002GL015578.
- Friedman, J. S. (2003), Tropical mesopause climatology over the Arecibo Observatory, *Geophys. Res. Lett.*, *30*(12), 1642, doi:10.1029/2003GL016966.
- Friedman, J. S., S. C. Collins, R. Delgado, and P. A. Castleberg (2002), Mesospheric potassium layer over the Arecibo Observatory,  $18.3^\circ\text{N}$ ,  $66.75^\circ\text{W}$ , *Geophys. Res. Lett.*, *29*(5), 1071, doi:10.1029/2001GL013542.
- Friedman, J. S., C. A. Tepley, S. Raizada, Q. H. Zhou, J. Hedin, and R. Delgado (2003), Potassium Doppler-resonance lidar for the study of the mesosphere and lower thermosphere at the Arecibo Observatory, *J. Atmos. Sol.-Terr. Phys.*, *65*, 1411–1424.
- Garcia, R. R. (1989), Dynamics, radiation and photochemistry in the mesosphere — implications for the formation of noctilucent clouds, *J. Geophys. Res.*, *94*, 14,605–14,615.
- Garcia, R. R., and S. Solomon (1985), The effect of breaking gravity waves on the dynamics and chemical composition of the mesosphere and lower thermosphere, *J. Geophys. Res.*, *90*, 3850–3868.
- Garcia, R. R., T. J. Dunkerton, R. S. Lieberman, and R. A. Vincent (1997), Climatology of the semiannual oscillation of the tropical middle atmosphere, *J. Geophys. Res.*, *102*(D22), 26,019–26,032.
- Gardner, C. S., X. Tao, and G. C. Papen (1995), Observations of strong wind shears and temperature enhancements during several sporadic Na layer events above Haleakala, *Geophys. Res. Lett.*, *22*, 2809–2812.
- Groves, G. V. (1972), Annual and semi-annual zonal wind components and corresponding temperature and density variations, 60–130 km, *Planet. Space Sci.*, *20*, 2099–2112.

- Höffner, J., and J. S. Friedman (2005), The mesospheric metal layer top-side: Examples of simultaneous metal observations, *J. Atmos. Sol. Terr. Phys.*, *67*, 1226–1237, doi:10.1016/j.jastp.2005.06.010.
- Holton, J. R. (1982), The role of gravity wave induced drag and diffusion in the momentum budget of the mesosphere, *J. Atmos. Sci.*, *39*, 791–799.
- Kawahara, T. D., T. Kitahara, F. Kobayashi, Y. Saito, A. Nomura, C.-Y. She, and D. A. Krueger (2002), Wintertime mesopause temperatures observed by lidar measurements over Syowa Station (69°S, 39°E), Antarctica, *Geophys. Res. Lett.*, *29*(15), 1709, doi:10.1029/2002GL015244.
- Kawahara, T. D., C. S. Gardner, and A. Nomura (2004), Observed temperature structure of the atmosphere above Syowa Station, Antarctica (69°S, 39°E), *J. Geophys. Res.*, *109*, D12103, doi:10.1029/2003JD003918.
- Leblanc, T., I. S. McDermid, P. Keckhut, A. Hauchecorne, C. Y. She, and D. A. Krueger (1998), Temperature climatology of the middle atmosphere from long-term lidar measurements at middle and low latitudes, *J. Geophys. Res.*, *103*(D14), 17,191–17,204.
- Lindzen, R. S. (1981), Turbulence and stress owing to gravity-wave and tidal breakdown, *J. Geophys. Res.*, *86*, 9707–9714.
- Lübken, F.-J., and U. von Zahn (1991), Thermal structure of the mesopause region at polar latitudes, *J. Geophys. Res.*, *96*(D11), 20,841–20,857.
- Meriwether, J. W., and C. S. Gardner (2000), A review of the mesosphere inversion layer phenomenon, *J. Geophys. Res.*, *105*(D10), 12,405–12,416.
- Meriwether, J. W., X. Gao, V. B. Wickwar, T. Wilkerson, K. Beissner, and S. Collins (1998), Observed coupling of the mesosphere inversion layer to the thermal tidal structure, *Geophys. Res. Lett.*, *25*, 1479–1482.
- Mlynczak, M. G., and S. Solomon (1993), A detailed evaluation of the heating efficiency in the middle atmosphere, *J. Geophys. Res.*, *98*, 10,517–10,541.
- Pan, W., and C. S. Gardner (2003), Seasonal variations of the atmospheric temperature structure at South Pole, *J. Geophys. Res.*, *108*(D18), 4564, doi:10.1029/2002JD003217.
- Pan, W., C. S. Gardner, and R. G. Roble (2002), The temperature structure of the winter atmosphere at South Pole, *Geophys. Res. Lett.*, *29*(16), 1802, doi:10.1029/2001GL014147.
- Picone, J. M., A. E. Hedin, D. P. Drob, and A. C. Aikin (2002), NRLMSISE-00 empirical model of the atmosphere: statistical comparisons and scientific issues, *J. Geophys. Res.*, *107*(A12), 1468, doi:10.1029/2002JA009430.
- Riese, M., D. Offermann, and G. Brasseur (1994), Energy released by recombination of atomic oxygen and related species at mesopause heights, *J. Geophys. Res.*, *99*, 14,585–14,593.
- Roble, R. G. (1995), Energetics of the mesosphere and thermosphere, the upper mesosphere and lower thermosphere: A review of experiment and theory, *Geophys. Monogr.*, *87*, 1–22.
- Sassi, F., and R. R. Garcia (1997), The role of equatorial waves forced by convection in the tropical semiannual oscillation, *J. Atmos. Sci.*, *54*(15), 1925–1942.
- Schmidlin, F. J. (1976), Temperature inversions near 75 km, *Geophys. Res. Lett.*, *3*, 173–176.
- She, C. Y., and J. R. Yu (1994), Simultaneous three-frequency Na lidar measurements of radial wind and temperature in the mesopause region, *Geophys. Res. Lett.*, *21*, 1771–1774.
- She, C. Y., and U. von Zahn (1998), Concept of a two-level mesopause: Support through new lidar observations, *J. Geophys. Res.*, *103*, 5855–5864.
- She, C. Y., J. R. Yu, and H. Chen (1993), Observed thermal structure of a midlatitude mesopause, *Geophys. Res. Lett.*, *20*, 567–570.
- She, C. Y., S. Chen, Z. Hu, J. Sherman, J. D. Vance, V. Vasoli, M. A. White, J. Yu, and D. A. Krueger (2000), Eight-year climatology of nocturnal temperature and sodium density in the mesopause region (80 to 105 km) over Fort Collins, CO (41°N, 105°W), *Geophys. Res. Lett.*, *27*, 3289–3292.
- Shepherd, M. G., W. F. J. Evans, G. Hernandez, D. Offerman, and H. Takahashi (2004), Global variability of mesospheric temperature: Mean temperature field, *J. Geophys. Res.*, *109*, D24117, doi:10.1029/2004JD005054.
- Shepherd, M. G., G. G. Shepherd, W. F. J. Evans, and S. Sridharan (2005), Global variability of mesospheric temperature: Planetary-scale perturbations at equatorial and tropical latitudes, *J. Geophys. Res.*, *110*, D24103, doi:10.1029/2005JD006128.
- Shepherd, M. G., G. Liu, and G. G. Shepherd (2006), Mesospheric semi-annual oscillation in temperature and nightglow emission, *J. Atmos. Sol. Terr. Phys.*, *68*, 379–389, doi:10.1016/j.jastp.2005.02.029.
- States, R. J., and C. S. Gardner (2000a), Thermal structure of the mesopause region (80–105 km) at 40°N latitude, Part I: seasonal variations, *J. Atmos. Sci.*, *57*, 66–77.
- States, R. J., and C. S. Gardner (2000b), Thermal structure of the mesopause region (80–105 km) at 40°N latitude, Part II: Diurnal variations, *J. Atmos. Sci.*, *57*, 78–92.
- Takahashi, H., B. R. Clemesha, and P. P. Batista (1995), Predominant semi-annual oscillation of the upper mesospheric airglow intensities and temperatures in the equatorial region, *J. Atmos. Sol. Terr. Phys.*, *57*(4), 407–414.
- Taylor, M. J., A. K. Taori, D. R. Hatch, H. L. Liu, and R. G. Roble (2005), Characterization of the semi-annual-oscillation in mesospheric temperatures at low-latitudes, *Adv. Space Res.*, *35*, 2037–2043, doi:10.1016/j.asr.2005.05.111.
- von Zahn, U., and J. Höffner (1996), Mesopause temperature profiling by potassium lidar, *Geophys. Res. Lett.*, *23*, 141–144.
- von Zahn, U., J. Höffner, V. Eska, and M. Alpers (1996), The mesopause altitude: only two distinctive levels worldwide?, *Geophys. Res. Lett.*, *23*, 3231–3234.
- Zhang, X., J. M. Forbes, M. E. Hagan, J. M. Russell III, S. E. Palo, C. J. Mertens, and M. G. Mlynczak (2006), Monthly tidal temperatures 20–120 km from TIMED/SABER, *J. Geophys. Res.*, *111*, A10S08, doi:10.1029/2005JA011504.

X. Chu, Cooperative Institute for Research in Environmental Sciences & Department of Aerospace Engineering Sciences, University of Colorado, Boulder, USA.

J. S. Friedman, NAIC Arecibo Observatory, Arecibo, Puerto Rico, USA. (jonathan@naic.edu)